

Nonequilibrium Phase Diagram of Sticky Nanotube Suspensions

E. K. Hobbie and D. J. Fry

National Institute of Standards and Technology, Gaithersburg, Maryland 20899, USA

(Received 9 February 2006; published 18 July 2006)

We report a universal phase diagram describing the evolution from solidlike networks to flowing nematics for “sticky” nanotube suspensions under an applied shear stress. Although the nanotubes are strongly non-Brownian, we find features characteristic of first-order phase transitions, including a discontinuity in the nematic order parameter at the isotropic-(para)nematic phase boundary. Using simple physical arguments, we account for the shape of the coexistence curves, as well as the dependence of the order parameter on concentration and stress.

DOI: [10.1103/PhysRevLett.97.036101](https://doi.org/10.1103/PhysRevLett.97.036101)

PACS numbers: 81.07.De, 82.70.Kj, 83.85.Ei

From actin in cells [1] to cellulose in paper [2], microscopic tubes and fibers impact our everyday lives in profound ways. They also offer the promise of new materials from carbon nanotubes [3–6] and new biotechnologies through the self-assembly of polypeptide chains [7]. Although aspect ratio and stiffness set such objects apart from other colloids and polymers, these qualities also create unique obstacles and challenges. Like flexible polymers, nanotubes and microfilaments are prone to mechanical entanglement, an effect compounded by attractive interactions. This strongly influences how such materials yield and flow in response to stress, impacting everything from the injection molding of carbon nanotube composites to the motility of living cells.

Beyond their contour length L and diameter d , nanotubes are characterized by a persistence length ξ_p , describing the decay of two-point correlations in segmental orientation along the backbone of the chain. For carbon nanotubes, in particular, ξ_p can be quite large, to the point where these objects can be effectively modeled as high-aspect-ratio rigid rods. Even with a surfactant coating, such extended objects are inherently sticky, and carbon nanotube suspensions typically form disordered networks or “gels” in equilibrium [8]. In this Letter, we report a generic phase diagram that maps the evolution from entangled networks to flow-induced nematics for sticky nanotube suspensions. The progression we find is hierarchical, with features characteristic of first-order phase transitions. Although the nanotubes are strongly non-Brownian, we find striking similarities with sheared suspensions of rod-like virus [9] and attractive colloids [10], with broad implications for controlling the morphology of nanotube networks. We also find nonlinear scaling between anisotropy and stress in agreement with a simple physical model.

We use multiwalled carbon nanotubes (MWNTs) grown via chemical vapor deposition, for which ξ_p is larger than L . From electron microscopy, $d \approx 50$ nm. The nanotubes were suspended in low-molecular-mass polyisobutylene (PIB) fluids using a polymeric dispersant [11]. Individual MWNTs in PIB are of sufficient length and contrast to be resolved in bright-field microscopy, and the mean L was

determined optically to be $10 \mu\text{m}$ ($L/d \approx 200$). The size distribution is nearly log-normal with a polydispersity of 2. We use two Newtonian fluids ($M_w = 500$ and $M_w = 800$) and an elastic fluid ($M_w = 800$ with 0.1% $M_w = 4.7 \times 10^6$). Suspensions (denoted $M1$, $M2$, and $M3$, respectively) were prepared at $\phi = 0.025\%$ to 10% MWNT by mass with $6 < cL^3 < 2500$ and $0.03 < cL^2d < 15$, where c is the number of MWNTs per unit volume, spanning the transition from semidilute to concentrated [12]. The overlap concentration, where $cL^3 \approx 1$, is 0.005% MWNT by mass. The nanotubes have an attractive interparticle potential of several $k_B T$ and flocculate in quiescence but can be fully dispersed with shear flow in the viscous solvents of interest here [11].

We consider linear shear flow along \hat{x} with a velocity gradient along \hat{y} and vorticity along \hat{z} . The strain rate is $\dot{\gamma} = \partial v_x / \partial y$ and we probe structure in the x - z plane at 25°C . Suspensions were homogenized at high $\dot{\gamma}$ and subjected to a decaying oscillatory shear flow to minimize hysteresis prior to measurement. Video microscopy, depolarized small-angle light-scattering [(SALS), $0.5 \mu\text{m}^{-1} < q < 5 \mu\text{m}^{-1}$ where q is the scattered wave vector], and flow birefringence measurements were performed in parallel-plate cells with variable gap, h . The shear stress, σ , the viscosity, η , the first normal stress difference, N_1 , and dynamic shear modulus, $G^*(\omega) = G'(\omega) + iG''(\omega)$, were measured in a controlled-strain cone-and-plate rheometer. A controlled-stress rheometer was used to measure $\eta(\gamma)$, where γ is the strain in response to an applied shear stress. For neat solvents, $\eta_s = 0.5$ Pa s for $M1$, $\eta_s = 10$ Pa s for $M2$, and $\eta_s = 10$ Pa s with $N_1 \approx 3.68 \dot{\gamma}^{2.38}$ (Pa) for $M3$, and isolated MWNTs deform at high $\dot{\gamma}$ [13].

Details of the rheology will be presented elsewhere and here we give just an overview [14]. Under steady shear flow, the viscosity shows dramatic and continuous shear thinning. Under small-amplitude oscillatory shear flow, $G^*(\omega)$ has a low-frequency plateau reflecting an elastic nanotube network [Fig. 1(a)]. From a scaling analysis of $G^*(\omega)$ [Fig. 1(b)], the shear modulus of the network (κ) as a function of nanotube concentration (ϕ) follows the simple power law $\kappa \propto \phi^\alpha$, with $\alpha \approx 7.1 (\pm 0.3)$ [suspension

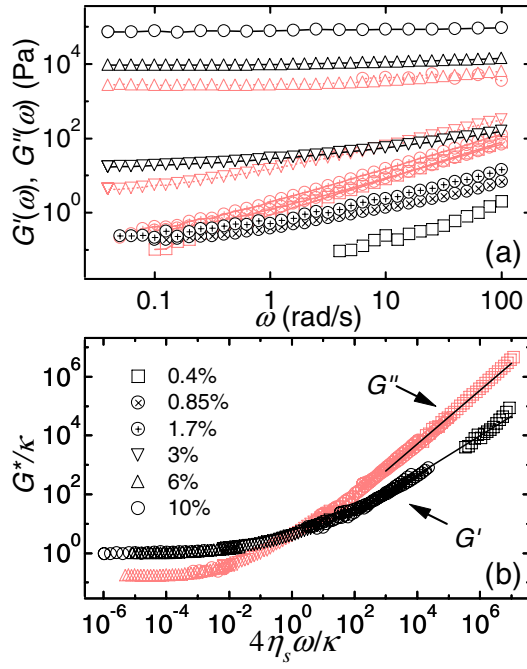


FIG. 1 (color online). (a) Loss (red) and storage (black) modulus for suspension M1 as a function of ϕ and ω and (b) scaling plot used to deduce $\kappa(\phi)$.

M1, Fig. 2(a)]. Controlled-stress measurements show the arrest of flow below a well defined yield stress, while above this threshold stress the suspensions flow indefinitely. All of these observations portray an elastic network of nanotubes that yields under sufficient force.

Large critical exponents are predicted for network elasticity [15] and simulations of rigid-rod networks in two dimensions suggest $\alpha = 6.7$ [16], remarkably close to the value we find above. Additionally, a simple scaling model of 3D fractal gels gives $\alpha = (3 + D_b)/(3 - D_f)$, where D_b and D_f are the backbone and network fractal dimension, respectively [17]. The exponent α is sensitive to D_f and would be smaller in suspensions with more open structures [18]. SALS measurements on homogenized suspensions show q^{-1} behavior, consistent with nominally straight nanotubes, while aggregated suspensions show q^{-D_f} at low q [Fig. 2(i)], with $D_f = 2.45(\pm 0.3)$. The dimension D_b —which describes the shape of the network backbone and is typically close to 1 [17]—cannot be deduced from SALS, but 5–100 \times digital microscopy gives the estimate $D_b \approx 1$, from which $\alpha = 7.1$ suggests $D_f \approx 2.44$. A recent study of diffusion-limited cluster aggregation for rigid rods [19] shows that D_f is an increasing function of L/d , and $D_f \approx 2.45$ is consistent with what we obtain by extrapolating the results in Ref. [19] to $L/d = 200$.

Connectivity of macroscopic clusters means that confinement is a critical factor and Fig. 3 shows the nonequilibrium “phase diagram” in the space of ϕ , h , and $\dot{\gamma}$. The highest concentration in Fig. 3 (3% M1) is close to where simple theory predicts a transition to a lyotropic nematic liquid crystal in monodisperse Brownian suspensions with

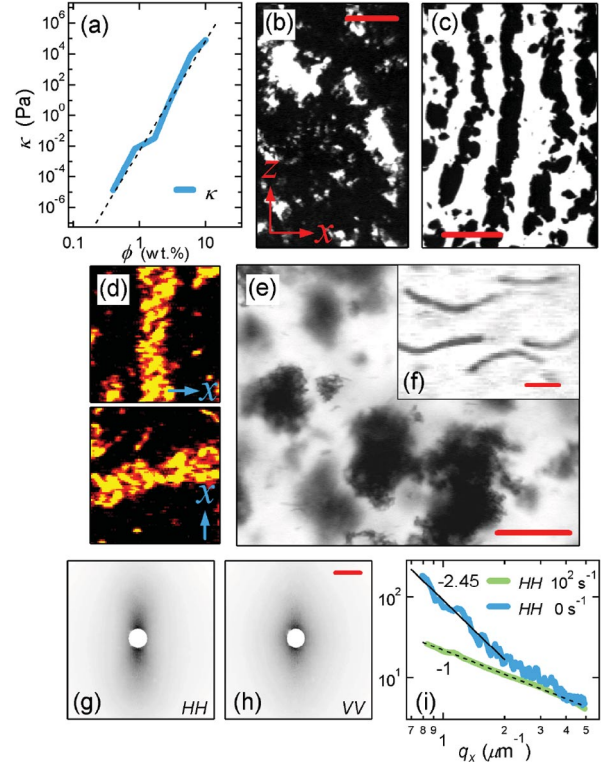


FIG. 2 (color online). (a) κ as a function of ϕ for M1; (b) cavitated network at 3% M1, 0.05 s⁻¹, and $h = 54 \mu\text{m}$ (bar = 150 μm); (c) striped pattern at 1.7% M1, 0.1 s⁻¹, and 125 μm (bar = 150 μm); (d) shear “band” in a thin sample rotated between crossed polarizers; (e) isolated aggregates at 0.1% M1, 2 s⁻¹, and 412 μm (bar = 40 μm); (f) flow-aligned MWNTs (bar = 5 μm); (g)–(h) light-scattering (SALS) patterns at 3% M1, 100 s⁻¹, and 54 μm where H denotes polarization along \hat{x} and V denoted polarization along \hat{z} (bar = 1 μm^{-1}); (i) SALS from dispersed and aggregated suspensions.

hard-rod interactions [20]. A dispersed flow-aligned state [Fig. 2(f)–2(h)] becomes unstable below a critical shear rate, $\dot{\gamma}_c$, giving way to aggregation [Fig. 2(e)]. This transition is ubiquitous, with $\dot{\gamma}_c$ increasing slightly with increasing ϕ . As $\dot{\gamma}$ decreases further, a periodic pattern of vorticity-aligned domains emerges [Fig. 2(c)]. Between crossed polarizers, these “bands” remain bright in rotated thin samples, suggesting an internal distribution of nanotube orientations with limited long-range anisotropy [Fig. 2(d)]. As ϕ increases further, the striped phase gives way to a cavitated network [Fig. 2(b)]. For 6% MWNT at $h = 30 \mu\text{m}$ the progression is similar. Phase boundaries are diffuse with coexistence, reminiscent of first-order phase transitions. The average $\dot{\gamma}$ where the arrest of flow occurs in stress-controlled measurements are below those in Fig. 3 (less than 10⁻² s⁻¹). A physical explanation is intuitive. Below a critical stress ($\sigma_c = \eta\dot{\gamma}_c$) there is insufficient force to break bonds between MWNTs contacted through the overlap of neighboring Jeffery orbits [21]. With increasing ϕ and decreasing σ , the size of these clusters increases. As weakly anisotropic objects, they

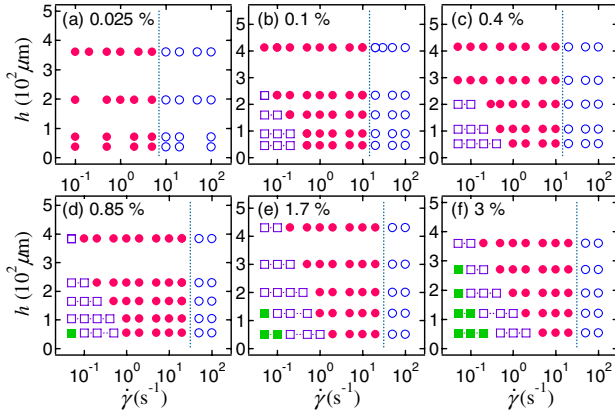


FIG. 3 (color online). Phase diagram of $M1$ in the parameter space of h , $\dot{\gamma}$, and ϕ deduced from controlled-strain optical and rheological measurements. Open circles are (para)nematics, closed circles are isolated aggregates, open squares are vorticity bands, and closed squares are cavitated networks. The vertical dashed line marks the stability limit.

move in Jeffery orbits of their own, but when the size becomes comparable to h , the orbits become confined to the x - z plane and the clusters floc end to end along \hat{z} into macroscopic bands. Periodicity arises from the growth of these bands at the expense of smaller clusters in their proximity. At still larger ϕ , macroscopic clusters become entangled, while under minimal stress, the quiescent network rearranges microscopically but remains otherwise intact.

We convert $\dot{\gamma}$ to σ using the measured viscosity. Dividing by σ_c then consolidates the horizontal axes in Fig. 3 on a dimensionless scale. To reduce h , we divide by the “equilibrium” mean cluster size $R_0(\phi)$, defined in the limit of small $\dot{\gamma}$, large h , and long time, to get the master plot in Fig. 4. The exponential growth of R_0 [Fig. 5(a)] reflects larger clusters sweeping out larger areas as they flow through the suspension, with $\delta R_0/\delta\phi \propto R_0$. Although data are shown for $M1$, similar behavior was observed for $M2$ and $M3$. The key difference is solvent viscosity, which shifts $\dot{\gamma}_c$ and alters the time scale for pattern formation, while σ_c itself is fairly insensitive to solvent type, being governed by the contact potential and friction between MWNTs [2]. As in a previous study [22], solvent elasticity had no apparent effect in the PIB fluids used here. The probability of finding a cluster of n nanotubes should decay exponentially in n/s for large n , where s is the mean cluster size [23]. From the definition of α given above, $s \propto \sigma^{-D_f/(3+D_b)} = \sigma^{-0.62}$. Since stripes form when clusters span the gap, the phase boundary for banding is simply a decaying exponential in $(\sigma/\sigma_c)^{0.62}$ (solid curve, Fig. 4).

In Fig. 4, the vertical line at $\sigma/\sigma_c \approx 1$ is the dispersion limit. By combining video microscopy, SALS, and flow birefringence [22], we measure the (para)nematic order parameter

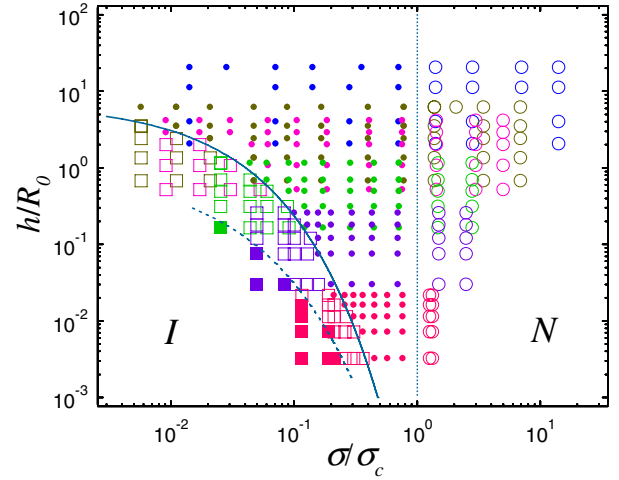


FIG. 4 (color online). Scaled phase diagram for the evolution from a solidlike disordered network (I) to a flowing nematic (N) for the data in Fig. 3, where concentration increases from top to bottom. Markers delineate the same morphologies as in Fig. 3, while colors denote concentration.

$$S = \langle P_2(\cos\theta) \rangle, \quad (1)$$

characterizing the degree of shear-induced alignment [Fig. 5(b)], where $P_2(\cos\theta) = \frac{1}{2}(3\cos^2\theta - 1)$ is the second Legendre polynomial and θ is the angle a nanotube makes

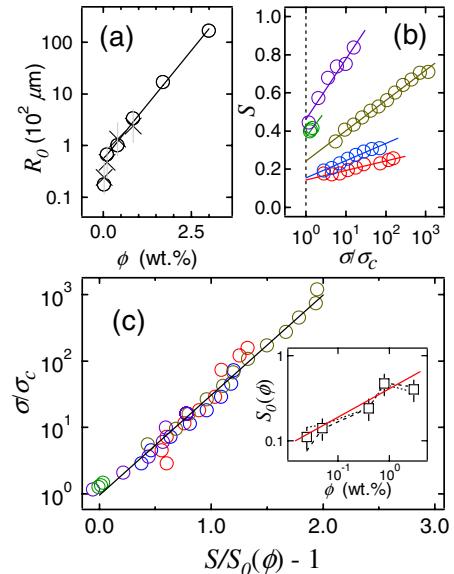


FIG. 5 (color online). (a) $R_0(\phi)$ for $M1$ with an exponential fit. Open circles are values empirically used to consolidate the vertical axes in Fig. 3 onto a single scale in Fig. 4 and hatched symbols are measured with optical microscopy. (b) S vs σ/σ_c with linear-log fits for 0.025% $M1$ (red), 0.05% $M1$ (blue), 0.4% $M3$ (brown), 0.8% $M3$ (purple), and 3.0% $M1$ (green). (c) σ/σ_c as a function of order parameter strain for the data in (b), where the inset shows $S_0(\phi)$. Dashed and dotted lines represent the intercept and slope from (b), respectively, and squares denote S_0 . The red line is a power law of $1/3$.

with the flow (x) direction. The discontinuity in S at σ_c is again suggestive of a first-order phase transition, and the intercept gives the order parameter at the dispersion limit, $S_0(\phi)$. The data in Fig. 5(b) suggest $S - S_0 \propto \ln(\sigma/\sigma_c)$, giving the scaling relation

$$\sigma/\sigma_c = \exp[a(S - S_0)/S_0] \quad (2)$$

shown in Fig. 5(c), with $a = 3.47$. This simple nonlinear constitutive equation relates the applied stress to an order parameter strain. On dimensional and physical grounds, $\delta S/\delta \dot{\gamma}$ is proportional to τ , the relaxation time for fluctuations in nanotube orientation. Taking τ as the period of a Jeffery orbit [21] ($\propto 1/\dot{\gamma}$) gives the observed logarithmic ordering. As shown in the inset to Fig. 5(c), the data suggest $S_0(\phi) \propto \phi^{1/3}$ for $\phi < 3\%$. To explain this, we expand Eq. (1) around the isotropic state $S = 0$. The brackets in Eq. (1) denote an average over the orientational distribution function, $p(\theta)$. Defining $\epsilon = \cos\theta - \frac{1}{\sqrt{3}}$, $\langle \epsilon \rangle$ scales as one over the average tube separation—or $\phi^{1/3}$ —in the semidilute regime. Expanding Eq. (1) in ϵ then gives the observed power law. Above 1%, the motion of adjacent MWNTs is correlated and this simple argument breaks down.

Signatures of first-order phase transitions in such a non-Brownian system are intriguing. The vertical axis in Fig. 4 is a measure of decreasing ϕ , and we compare our results with those recently reported for sheared suspensions of rodlike virus [9]. Beyond the non-Brownian nature of the MWNTs [14], a critical difference is the lack of a quiescent nematic phase, which is preempted here by a disordered network. A generic feature of long carbon nanotubes [24], our results demonstrate how this tendency for entanglement can be overcome at high shear stress, even in concentrated suspensions. Extending the biphasic regime in Ref. [9] to higher ϕ , some similarities start to emerge, with a first-order (binodal) line marking the limit of homogeneous dispersion. The different banding scenarios might simply reflect the different rheology of the dispersed phase; an isotropic gel compared to a nematic liquid crystal.

Finally, our results are reminiscent of those recently reported for colloidal suspensions with attractive interactions [10], Fig. 4 being a two-dimensional (σ - ϕ) slice at fixed interaction potential of an analogous three-dimensional phase diagram. The progression we observe, from a nonflowing disordered solid to a dispersed fluid, is typical of such “jammed” systems [10], which can form the same striped periodic patterns in confinement, albeit at much higher ϕ than reported here [25]. Our generalization of these results to anisotropic particles has far-reaching implications, but particularly for the flow processing of melt carbon nanotube composites [4–6,11], where it is essential to transport material with minimal shear stress, but with the rapid restoration of percolation in quiescence. The ability to tune and control topological interactions in diffuse networks of electrically conductive nanotubes cre-

ates a host of new opportunities in the realm of sensors, switches and mechanically responsive materials.

The authors thank E. A. Grulke for supplying the MWNTs and S. D. Hudson and D. J. Klingenberg for useful discussions.

-
- [1] M. L. Gardel *et al.*, *Science* **304**, 1301 (2004).
 - [2] C. F. Schmid and D. J. Klingenberg, *Phys. Rev. Lett.* **84**, 290 (2000).
 - [3] R. H. Baughman, A. A. Zakhidov, and W. A. de Heer, *Science* **297**, 787 (2002).
 - [4] B. Vigolo *et al.*, *Science* **309**, 920 (2005).
 - [5] M. B. Bryning *et al.*, *Adv. Mater.* **17**, 1186 (2005).
 - [6] T. Chatterjee *et al.*, *Adv. Funct. Mater.* **15**, 1832 (2005).
 - [7] B. Ozbas *et al.*, *Phys. Rev. Lett.* **93**, 268106 (2004).
 - [8] L. A. Hough *et al.*, *Nano Lett.* **6**, 313 (2006).
 - [9] M. P. Lettinga and J. K. G. Dhont, *J. Phys. Condens. Matter* **16**, S3929 (2004).
 - [10] V. Trappe *et al.*, *Nature (London)* **411**, 772 (2001).
 - [11] S. Lin-Gibson *et al.*, *Phys. Rev. Lett.* **92**, 048302 (2004).
 - [12] M. Doi and S. F. Edwards, *The Theory of Polymer Dynamics* (Oxford University, New York, 1986).
 - [13] The deformation of comparable MWNTs has been measured [M. F. Yu *et al.*, *Science* **287**, 637 (2000)]. The Young’s modulus is $E_Y \approx 40$ GPa and the bending stiffness is $B = E_Y \pi d^4 / 2^6 \approx 1.22 \times 10^{-20}$ N m². For $M1$, the dimensionless bending stiffness, $B/(\eta_s \dot{\gamma} L^4)$, and bending ratio, $E_Y [\ln(2r_e) - 1.5] d^4 / (2\eta_s \dot{\gamma} L^4)$, where $r_e = 1.24(L/d)/[\ln(L/d)]^{1/2}$, are 0.02 and 0.5, respectively, at 100 s⁻¹. For dimensionless bending ratios less than 1, the tubes will deform.
 - [14] At the smallest $\dot{\gamma}$, the bare rotational Peclet number, $Pe = \pi \eta_s L^3 \dot{\gamma} / 3k_B T [\ln(L/d) - 0.8]$, is much larger than 1, and the MWNT suspensions are non-Brownian. The Reynolds number, $Re = \dot{\gamma} h^2 \rho / \eta_s$ where ρ is the solvent mass density, is always much less than 1, while the Weissenberg number, $Wi = N_1/\sigma$, is typically larger than 1 in magnitude, implying that elasticity is important.
 - [15] Y. Kantor and I. Webman, *Phys. Rev. Lett.* **52**, 1891 (1984).
 - [16] J. Wilhelm and E. Frey, *Phys. Rev. Lett.* **91**, 108103 (2003).
 - [17] W.-H. Shih *et al.*, *Phys. Rev. A* **42**, 4772 (1990).
 - [18] L. A. Hough *et al.*, *Phys. Rev. Lett.* **93**, 168102 (2004).
 - [19] A. Mohraz *et al.*, *Phys. Rev. Lett.* **92**, 155503 (2004).
 - [20] G. J. Vroege and H. N. W. Lekkerkerker, *Rep. Prog. Phys.* **55**, 1241 (1992).
 - [21] The dispersed nanotubes are observed to be in periodic orbits around \hat{z} , as first derived by Jeffery [G. B. Jeffery, *Proc. R. Soc. A* **102**, 161 (1922)].
 - [22] D. Fry *et al.*, *Phys. Rev. Lett.* **95**, 038304 (2005).
 - [23] P. Meakin and M. H. Ernst, *Phys. Rev. Lett.* **60**, 2503 (1988).
 - [24] W. Song, I. A. Kinloch, and A. H. Windle, *Science* **302**, 1363 (2003).
 - [25] A. Montesi, A. A. Pena, and M. Pasquali, *Phys. Rev. Lett.* **92**, 058303 (2004).